Applied Catalysis B: Environmental 127 (2012) 89–98

Contents lists available at SciVerse ScienceDirect

Applied Catalysis B: Environmental

journal homepage: www.elsevier.com/locate/apcatb

Effect of calcium dopant on catalysis of Ir/La_2O_3 for hydrogen production by oxidative steam reforming of glycerol

Guangxing Yang, Hao Yu*, Xiaoya Huang, Feng Peng*, Hongjuan Wang

School of Chemistry and Chemical Engineering, South China University of Technology, Guangzhou 510640, China

ARTICLE INFO

Article history:
Received 25 April 2012
Received in revised form 4 August 2012
Accepted 9 August 2012
Available online 16 August 2012

Keywords:
Iridium
$La_2O_2CO_3$
Reforming
Glycerol
Calcium

ABSTRACT

The superfluous glycerol derived from biodiesel production can be a low-cost feedstock for hydrogen production via reforming technology. In this work, a La_2O_3 supported iridium catalyst was employed to catalyze the oxidative steam reforming of glycerol (OSRG) for hydrogen production, in the range of S/C ratio of 1–3, C/O ratio of 0.75–1 and 550–750 °C. The catalyst was modified with Na, Mg and Ca to optimize the catalytic performance in OSRG reaction. It was found that Ca is promising in promoting Ir/La_2O_3 catalyst for OSRG, offering excellent activity, hydrogen selectivity and stability. By combining multiple techniques, i.e. XRD, FTIR, Raman, XPS, H_2-TPR, CO_2-TPD and HRTEM, the Ca modified Ir/La_2O_3 catalyst was characterized to understand the role of Ca promoter. Multi-functions of Ca were demonstrated, including inducing structural defects of $La_2O_2CO_3$, endowing the catalyst strong basicity and tuning the metal–support interaction, which make the catalyst highly resistant to coking and sintering, therefore performing excellent long-term stability for 100 h.

1. Introduction

Biodiesel, as an important biofuel alternative, has been produced massively by transesterification of vegetable oils and animal fats, meanwhile about 10 wt% of glycerol is produced as a byproduct. Because of the rapid growth of global production projection of biodiesel driven by mandatory environmental regulations [1], it is highly desired to develop new derivates from glycerol building block [2]. In energy sector, the superfluous glycerol can be a low-cost feedstock for hydrogen or synthesis-gas production via reforming technology, which has been proved feasible in terms of thermodynamics and experiments [3,4].

Hydrogen or syngas can be generated from glycerol by steam reforming (SR) [5–7], aqueous-phase reforming (APR) [8], pyrolysis [9], supercritical water reforming [10], and photo-reforming [11]. So far, the thermal reforming approach is most extensively studied for abstracting hydrogen from glycerol. To reduce the energetic requirement of the endothermic reaction, oxygen can be added into the feedstock to supply the energy via burning some glycerol. The overall reaction of oxidative steam reforming of glycerol (OSRG) is:

$$C_3H_8O_3(g) + (3-2\delta)H_2O(g) + \delta O_2(g) \rightarrow 3CO_2(g) + (7-2\delta)H_2(g) \quad (1)$$

In addition, the introduction of oxygen in the system can inhibit some undesired reactions, e.g. carbon deposition, at the expense of H_2.

Most catalysts succeeded in the reforming of methanol, ethanol and other carbohydrates can be applied to catalyze the reforming reaction of glycerol, due to chemical similarity of feedstocks. These catalysts include nickel-based, cobalt-based and noble metal catalysts, etc. Supported Ni catalysts have been widely investigated in most carbohydrate reforming reactions due to its ability to break C—C bond and inexpensiveness. Hydrogen can be produced by SR of glycerol over Ni supported on Al_2O_3, CeO_2, MgO, TiO_2, SiO_2, ZrO_2 and La_2O_3 [5,6,12–14]. Ni/Al_2O_3 catalyst performed efficiently in high H_2 selectivity and glycerol conversion [12–14]. However, Ni catalysts frequently suffer from deactivation caused by carbon deposition on catalyst surface, which blocks active sites and increases the concentrations of by-products, such as methane and ethylene [15,16]. Modifying Al_2O_3 with La_2O_3, CeO_2, MgO and ZrO_2 can improve the catalytic activity and stability for SRG via preventing Ni from incorporation to Al_2O_3 phase [17], stabilizing Ni^0 particles [18] and reducing support acidity [6–19]. It is also cognized that the catalytic activity may be enhanced by modifying Ni catalysts with a small quantity of noble metal, such as Pt [19] and Pd [20,21]. For the case of Co catalysts [22–24], it was evident that carbon deposits on the catalyst even under excess steam-to-carbon ratios [22]. Pereira et al. reported that adding 1% Ru and 0.5% Na effectively improved the activity and stability of Co/Al_2O_3 catalyst in the oxidative steam reforming of a glycerol–ethanol mixture [23]. In their work, a 12-day stability was achieved by

* Corresponding authors. Tel.: +86 20 8711 4916; fax: +86 20 8711 4916.
E-mail addresses: yuhao@scut.edu.cn (H. Yu), cefpeng@scut.edu.cn (F. Peng).

0926-3373/$ – see front matter © 2012 Elsevier B.V. All rights reserved.
http://dx.doi.org/10.1016/j.apcatb.2012.08.003

suppressing coking at 648 K, S/C = 2, (glycerol + EtOH)/O_2 = 2, and GHSV = 3900 h^{-1}.

Noble metals, such as Pt [25–28], Rh [12,16,26,29,30], Ru [7,31,32] and Ir [33], display excellent catalytic performances in glycerol reforming. Compared with base metals, supported noble metal catalysts provide near-equilibrium product distribution under similar reaction conditions [34]. With highly active Rh-Ce/Al_2O_3 catalyst, the reactor can be operated at a short contact time about 10 ms [26]. Despite of the high activity, noble metal catalysts suffer from deactivation caused by coking and sintering in the process of SR and APR of glycerol [16,27]. Although co-feeding oxygen can reduce carbon formation on the surface of catalyst, a long-term stability test of Rh/Al_2O_3 catalyst in OSRG reaction revealed severe coking and active metal sintering at high temperatures in the oxidation zone of reactor, resulted in ca. 40% decrease in hydrogen production during 100 h time on stream [30].

In the reforming system, coke can be formed via irreversible side reactions, e.g. CO disproportionation, methane decomposition and polymerization. The rate of coke formation strongly depends on design of catalyst composition and its structural control. For example, coking can be suppressed as the size of nickel particles was well controlled [35–37], emphasizing the necessity of preventing thermal-sintering in the high-temperature reaction. Recently, we found that $La_2O_2CO_3$ supported iridium catalyst is efficient and stable in OSR of ethanol [38]. $La_2O_2CO_3$ stabilizes metal particles via (i) dynamic dissolution and exsolution of Ir in support to prevent thermal sintering; and (ii) the following reactions to gasify carbon deposits [39,40]:

$$La_2O_3 + CO_2 \leftrightarrow La_2O_2CO_3 \quad (2)$$

$$La_2O_2CO_3 + C \rightarrow La_2O_3 + 2CO \quad (3)$$

In this work, the La_2O_3 supported iridium catalyst was employed to catalyze OSRG reaction for hydrogen production. The catalyst was modified with alkali metals to optimize the catalytic performance in OSRG reaction. One of the major concerns was on preventing the deactivation attributed to coking and sintering. It was found that Ca can be a prospective promoter of Ir/La_2O_3 catalyst for OSRG, displaying excellent activity, hydrogen selectivity and stability.

2. Experimental

2.1. Catalyst preparation

Iridium catalysts were prepared by impregnating oxide supports with appropriate amounts of iridium aqueous solution ($IrCl_3$ $4H_2O$, Ir content: 54.51 wt%, Shanghai July Chemical Co., Ltd, China). The slurry was dried at 120 °C over night, and then calcined at 500 °C in air for 2 h. The resulting catalysts were denoted as Ir(x)/La_2O_3, where x is the nominal weight percentage of Ir in catalysts. Although La_2O_3 converts to $La_2O_2CO_3$, $La(OH)_3$ or their mixture during reaction, as discussed below, we named the catalysts with La_2O_3 for simplicity unless otherwise mentioned. An Ir/$CaCO_3$ catalyst was prepared with the same method by replacing La_2O_3 with CaO.

The Ir(x)/La_2O_3 catalyst was modified with Na, Mg and Ca by a two-step impregnation method. The promoter was firstly introduced into La_2O_3 by wetness impregnation with an aqueous solution of nitrates, e.g. $NaNO_3$, $Mg(NO_3)_2$, $Ca(NO_3)_2{\cdot}4H_2O$. The slurry was dried at 120 °C over night, and then calcined at 500 °C in air for 2 h. Iridium was subsequently loaded with the aforementioned method but using the modified La_2O_3 as support. The modified catalysts were denoted as Ir(x)M(y)/La_2O_3, where x is the nominal weight percentage of Ir, y is the nominal weight percentage of promoting metal in catalysts and M = Na, Mg, Ca.

2.2. Catalytic test

OSRG reactions were performed in a quartz fixed-bed reactor with inner diameter of 8 mm. In each experiment, 0.2 g catalyst was sandwiched by quartz wool and packed in reactor. A thermocouple was inserted into the center of the catalytic bed to monitor and control the reaction temperature. The mixture of glycerol and water was fed into the upper of catalyst bed by a syringe pump though a stainless steel capillary tube (0.3 mm in inner diameter). O_2 was introduced into reactor from a Ø 3 mm stainless steel tube around the capillary tube to avoid early mixing between O_2 and glycerol and resultant homogeneous combustion. Before reaction, the catalyst was activated with H_2 at a flow rate of 50 ml/min at 500 °C for 45 min. The gas off the reactor passed though an ice-water cold trap to condense the unreacted glycerol and water. The condensate liquid was collected at certain time intervals for measuring glycerol conversion.

The reformate gas was analyzed by a gas chromatograph equipped with a thermal conductivity detector (TCD) and a flame ionization detector (FID). A TDX 01 column was used for H_2 analysis in TCD. CO, CH_4, CO_2 and C_2H_4 were analyzed by FID with a packed column for analyzing transformer oil. CO and CO_2 were converted to methane in a methanator packed with Ni catalyst before entering FID. The concentration of glycerol in condensate liquid was analyzed by a high performance liquid chromatograph equipped with a refractive index detector.

The average glycerol conversion within a time interval of 30–60 min was calculated by

$$\bar{X} = \frac{\text{moles of glycerol feeded} - \text{moles of glycerol in liquid}}{\text{moles of glycerol feeded}} \times 100\%$$

The selectivity of H_2 was calculated by

$$S_{H_2} = \frac{\text{moles of } H_2 \text{ produced}}{\text{moles of carbon in gas product}} \times \frac{3}{4} \times 100\%$$

The selectivity of carbon containing species (CO, CO_2, CH_4 and C_2H_4) in gas products were calculated by

$$S_i = \frac{n \times \text{moles of } i}{\text{moles of carbon in gas product}} \times 100\%$$

where n is the atom number of carbon in i species.

2.3. Catalyst characterizations

Since La_2O_3 tends to form hydrated $La_2(CO_3)_3$ when exposed in damp air [41], the reduced or used samples were cooled down to room temperature in N_2 atmosphere and sealed in dry air prior to characterizations. Specific surface areas of catalysts were measured by N_2 adsorption at 77 K (ASAP 2010, Micromeritics). Before the measurement, the samples were degassed at 573 K under vacuum over night. XRD patterns were obtained with an Shimadzu XD-D1 instrument using Cu Kα radiation at 35 kV and 40 mA. The scan rate was 1° min^{-1} from 10° to 60°. The FT-IR spectra were obtained using a Nicolet 380 FT-IR spectrometer with a spectral resolution of 4 cm^{-1} by pelletizing catalysts with KBr (ca. 2 wt% catalyst in a pellet). Raman scattering spectra were recorded with a Renishaw RM2000 spectrometer excitated at 514.5 nm. X-ray photoelectron spectroscopy (XPS) was performed with a Kratos Axis ultra spectrometer excited with Al Kα X-ray source. The binding energies (±0.2 eV) were referenced to C_{1s} peak of adventitious carbon at 284.6 eV. High resolution transmission electron microscopy (HRTEM) images were obtained in JEM-2010/2010F (JEOL) microscopes equipped with an INCA energy dispersive spectrometer (Oxford Instruments) operated at 200 kV. Specimens for HRTEM were prepared by ultrasonically suspending the sample in acetone and depositing a drop of the suspension onto a copper grid covered

by amorphous carbon. H_2 temperature-programmed reduction (TPR) was carried out in an Auto Chem II Chemisorption Analyzer. Before H_2-TPR experiments, ca. 0.15 g fresh catalyst was pretreated in Ar at 500 °C for 0.5 h. Then the TPR profile was recorded from 50 to 800 °C at a ramping rate of 10 °C min^{-1} under flowing H_2(10%)/Ar at 50 Ncm^3 min^{-1}. CO_2 temperature-programmed desorption (CO_2-TPD) was carried out in a TP5080 adsorption instrument. Before CO_2-TPD experiments, 0.02 g fresh supports were pretreated in He at 650 °C for 0.5 h. And then these samples were exposed in CO_2 atmosphere for 2 h. Then the TPD profiles were recorded from room temperature to 900 °C at a ramping rate of 10 °C min^{-1} under flowing He at 50 Ncm^3 min^{-1}.

3. Results and discussion

3.1. OSRG performance of Ir/La_2O_3 catalyst

As shown in Table 1, the catalytic performance of iridium catalysts supported on La_2O_3, γ-Al_2O_3 and CeO_2, were compared. Except for the products presented in Table 1, there were other by-products, such as acetaldehyde and acetone, in condensate liquid. But they were in traces therefore not measured for analysis. On the most commonly used support, γ-Al_2O_3, the iridium catalyst displayed the highest conversion. However, the H_2 selectivity was quite low, associated with relatively high C_2H_4 selectivity, indicating coking caused by polymerization over the acidic sites of support. CeO_2 is widely used as support in reforming, oxidation and water gas shift, due to its oxygen storage ability. The H_2 selectivity was low over CeO_2, while CO_2 selectivity was higher than Al_2O_3 supported catalyst, suggesting the oxygen storage may facilitate the formation of CO_2 and water. Although the conversion of glycerol over Ir/La_2O_3 was slightly lower than the catalysts supported on γ-Al_2O_3 and CeO_2, it offered much higher H_2 selectivity. With 3 wt% loading of Ir, 62.5% H_2 selectivity, 3–folds of that over Ir/γ-Al_2O_3, was achieved. The conversion slightly decreased with the increase of Ir loading. The maximum H_2 selectivity was reached over the catalysts with Ir loading ranging from 3 to 5%. The high Ir loading above 7 wt% resulted in substantial C_2H_4 yield, exposing the catalyst to the risk of coking. Thus, a decrease of H_2 selectivity by ca. 30% was observed during the first 200 min over $Ir(9)/La_2O_3$ (not shown).

We performed a parametric study for the OSRG process with $Ir(3)/La_2O_3$ catalyst. As shown in Table 2 (entries 1–3), although increased conversion, the H_2 selectivity decreased with decreasing C/O ratio, defined as the molar ratio of carbon in feed to oxygen in O_2 introduced, due to the combustion reaction. The conversion and H_2 selectivity both increased with S/C ratio, defined as the molar ratio of steam to carbon in feed, because the hydrogen in water may contribute to the H_2 production via WGS reaction (entries 2, 4, 5), and the formation of coke can be suppressed, indicated by the lower selectivity of C_2H_4 at high S/C. Higher reaction temperatures facilitated the conversion and hydrogen yield. However, undesired C_2H_4 also increased with reaction temperature (entries 2, 6, 7). The investigation on space velocity (entries 2, 8, 9) shows that the lower GHSV is beneficial for hydrogen yield, while produces more C_2H_4. Above results are well consistent with our previous thermodynamic study [34].

The Ir/La_2O_3 catalyst has shown excellent activity and stability in OSR reaction of ethanol. With optimized catalyst formulation and reaction conditions, high efficiency hydrogen production has been proven over 300 h time on stream without deactivation [38]. Unfortunately, the Ir/La_2O_3 catalyst failed to extend this stable performance to OSRG reaction. As shown in Fig. 1, a short-term stability test shows that the H_2 selectivity decreased by ca. 25% from 65.4% to 39.9% within ca. 8 h on stream. Meanwhile, the selectivities of CO, CH_4 and C_2H_4 increased. The formation of coke is one of the reasons for the deactivation. As shown in Fig. 2, the Raman scattering spectrum of the used Ir (3)/La_2O_3 catalyst definitely indicates the formation of carbon on catalyst surface, characterized by the strong G and D bands of carbon at 1596 and 1341 cm^{-1}, respectively. These results imply that the C—C bond breakage is more challenging in the case of glycerol reforming compared to ethanol. Such an effect can be expected to be resulted from the mismatch of the kinetics of elementary steps of OSRG reaction, e.g. fast coking and strong adsorption of intermediates, since from the point of view of thermodynamics, glycerol has lower potential to form solid carbon in OSRG [34]. Thus, a further modification on the Ir/La_2O_3 catalyst is desired.

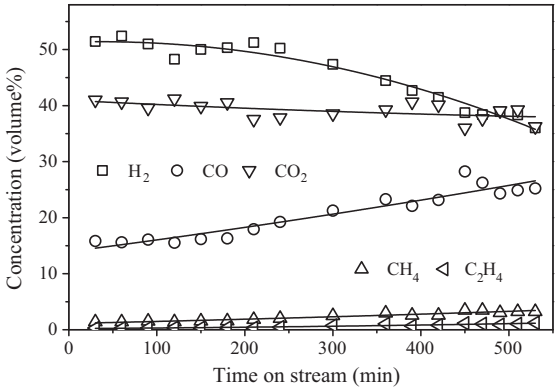

Fig. 1. Short-term stability of product selectivity over $Ir(3)/La_2O_3$ catalyst in OSRG reaction. Reaction condition: C/O = 1, S/C = 2, T = 650 °C, GHSV = 120,000 h^{-1}.

3.2. Effect of modifier on OSRG performance of Ir/La_2O_3

Alkaline and alkaline earth metals are widely used to modify solid catalysts to suppress coking via increasing catalyst basicity [42–46]. In this work, Na, Mg and Ca were investigated as modifiers of Ir catalyst. They were regarded as alkaline promoters to prevent catalyst from coking. In addition, they were expected to tune the interaction between metal and support, thereby inhibiting sintering of catalyst [47,48].

Table 3 shows the effects of Na, Mg and Ca on the catalytic performances of $Ir(3)/La_2O_3$ catalyst. The three modifiers, in 1 wt% content, slightly improved glycerol conversion under the same condition. Meanwhile, substantial elevations in H_2 selectivity were observed over the Ca promoted catalyst. More importantly, in short-term stability tests, all the modified catalysts exhibited

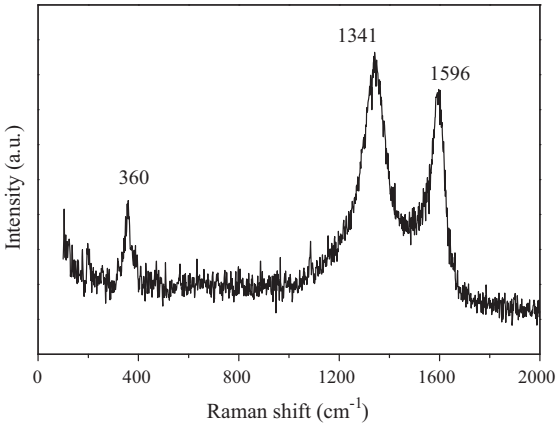

Fig. 2. Raman scattering spectrum of used $Ir(3)/La_2O_3$ catalyst. Reaction condition: C/O = 1, S/C = 2, T = 650 °C, GHSV = 120,000 h^{-1}, 8.7 h.

Table 1
OSRG performance of Ir catalysts supported on various oxides. Conditions: S/C = 2, C/O = 1, GHSV = 120,000 h^{-1}, T = 650 °C. All the data were taken at reaction time of about 200 min.

Catalyst	Conversion (%)	Selectivity (%)				
		H_2	CO	CH_4	CO_2	C_2H_4
Ir(3)/γ-Al_2O_3	81.4	19.5	39.9	3.7	50.1	5.0
Ir(3)/CeO_2	79.3	24.6	30.7	4.5	62.8	3.5
Ir(1)/La_2O_3	79.0	47.4	25.7	3.1	70.4	2.3
Ir(3)/La_2O_3	79.1	62.5	31.9	3.3	63.2	1.5
Ir(5)/La_2O_3	76.7	61.2	27.0	3.3	67.7	1.5
Ir(7)/La_2O_3	77.0	43.3	28.8	3.1	64.0	3.4
Ir(9)/La_2O_3	72.0	59.6	44.8	9.8	28.4	15.1

Table 2
Parametric study of OSRG reaction over Ir(3)/La_2O_3 catalyst. All the data were taken at reaction time of about 200 min.

Entry	S/C	C/O	T (°C)	GHSV (h^{-1})	Con. (%)	Selectivity (%)				
						H_2	CO	CH_4	CO_2	C_2H_4
1	2	1.5	650	120,000	67.0	72.3	36.0	3.9	56.8	2.5
2	2	1	650	120,000	79.1	62.5	31.9	3.3	63.2	1.5
3	2	0.75	650	120,000	81.0	45.5	25.8	2.6	69.4	1.8
4	1	1	650	120,000	76.0	50.0	30.6	4.2	64.4	3.2
5	3	1	650	120,000	81.0	62.7	28.0	2.4	66.2	0.6
6	2	1	550	120,000	71.3	32.6	26.0	2.4	69.3	1.9
7	2	1	750	120,000	82.0	84.2	48.6	9.3	36.3	6.9
8	2	1	650	60,000	78.5	81.2	32.4	4.8	58.8	2.8
9	2	1	650	180,000	73.5	51.2	26.2	2.1	69.8	0.7

improved stability allowing for hydrogen production without any loss of conversion and H_2 selectivity for ca. 8 h (see Fig. S1 in supporting information), suggesting that the catalytic performance of Ir(3)/La_2O_3 catalyst may be tuned by alkaline and alkaline earth metals. As predicted, such an enhancement is probably linked to the coking inhibition by increased alkality, indicated by the reduced C_2H_4 selectivity.

Among the three modifiers, the calcium promoted catalyst displayed the highest activity and H_2 yield, thus we optimized the formulation of Ir(3)Ca(y)/La_2O_3 catalyst. As shown in Table 3, the highest catalytic activity for OSRG was obtained over the catalysts with 5–9 wt% Ca, meanwhile the hydrogen selectivity was up to 74.5%. Further increasing Ca content to 15% led to a sharp decrease of OSRG performance, especially in rapid deactivation within 8 h on stream (see Fig. S2 in supporting information), probably due to the formation of coke. The long-term stability test of Ir(3)Ca(9)/La_2O_3 catalyst is shown in Fig. 3. There were no obvious changes in conversion and product concentrations during 100 h on stream, indicating the improved stability of Ir(3)Ca(9)/La_2O_3 compared with the pristine Ir(3)/La_2O_3 catalyst. Such a stable performance is a substantial improvement on the stable hydrogen production from glycerol, compared to state-of-the-art catalysts for either SR or OSR of glycerol in literatures [16,30].

Table 3
OSRG performance of Na, Mg, Ca modified Ir(3)/La_2O_3 catalysts. Conditions: S/C = 2, C/O = 1, GHSV = 120,000 h^{-1}, T = 650 °C. All the data were taken at reaction time of about 400 min.

Modifier	Conversion (%)	Selectivity (%)				
		H_2	CO	CH_4	CO_2	C_2H_4
Na (1 wt%)	81.2	61.3	28.8	2.5	66.8	1.6
Mg (1 wt%)	79.8	57.6	25.9	3.9	67.4	2.2
Ca (1 wt%)	82.3	67.5	25.6	2.5	70.3	1.2
Ca (3 wt%)	78.8	70.2	28.7	2.1	67.7	1.3
Ca (5 wt%)	88.4	71.5	27.0	2.2	69.5	1.2
Ca (9 wt%)	87.2	74.1	29.5	2.3	66.2	1.3
Ca (15 wt%)	82.1	50.1	30.3	7.1	55.5	5.5

3.3. Characterizations of Ir (3)Ca(y)/La_2O_3 catalysts

In the present work, we characterized the Ca-promoted catalysts with multiple techniques to understand the role of Ca in the iridium-catalyzed OSRG reaction. It should be noted that Na and Mg are also effective as promoters. However, on current stage, the study was focused on Ca and the investigation on the other promoters was left open, due to the superior performance of Ca-promoted catalysts.

Fig. 4a–c shows the XRD patterns of as-prepared, reduced and used Ir (3)Ca(y)/La_2O_3 catalysts. In all of the patterns, reflections from Ir species are absent, because: (i) Ir loadings are low; (ii) highly dispersed Ir species may be formed, and (iii) strong interaction leads to the formation of mixed oxides. However, a wealth of information on supports and their evolution is revealed. The as-prepared Ir(3)Ca(y)/La_2O_3 catalysts are composed of La_2O_3, $La(OH)_3$ and hexagonal and monoclinic $La_2O_2CO_3$. La_2O_3 and $CaCO_3$ can only be detected in the samples with more than 5 wt% of Ca. The major crystalline phase in support is $La_2O_2CO_3$. Increasing Ca content

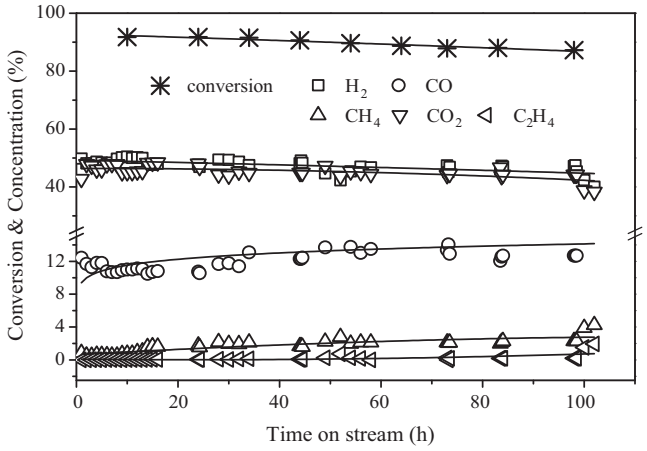

Fig. 3. Stability of Ir(3)Ca(9)/La_2O_3 catalyst in OSRG reaction. Reaction condition: C/O = 1, S/C = 2, T = 650 °C, GHSV = 60,000 h^{-1}.

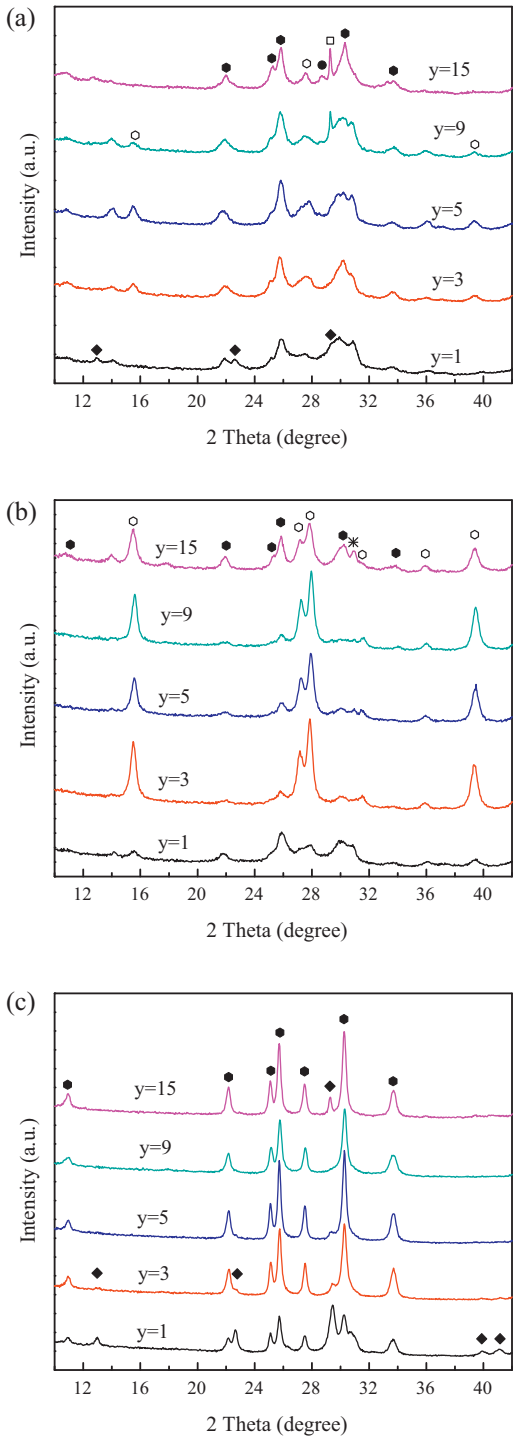

Fig. 4. XRD patterns of as-prepared (a), reduced (b) and used (c) Ir(3)Ca(y)/La_2O_3 catalysts. Reaction condition: C/O = 1, S/C = 2, T = 650 °C, GHSV = 60,000 h^{-1}, reaction time of about 8 h. Legend: ● – La_2O_3 (JCPDS 831355); ⬢ – hexagonal (type II) $La_2O_2CO_3$ (JCPDS 841963); ♦ – monoclinic (type I) $La_2O_2CO_3$ (JCPDS 481113); ⬡ – $La(OH)_3$ (JCPDS 832034); □ – $CaCO_3$ (JCPDS 851108); * – La_2CaO_x (JCPDS 420342).

facilitates the dioxycarbonate to transform into its thermodynamically stable phase, hexagonal (type II) $La_2O_2CO_3$ [41]. Reduction in H_2 makes the mixed La species converted to La $(OH)_3$ and hexagonal $La_2O_2CO_3$. In the XRD patterns of Ir(3)Ca(3–9)/La_2O_3, the main reflections are from $La(OH)_3$. Increasing Ca content to 15% leads to the stronger reflections of $La_2O_2CO_3$, meanwhile calcium-containing mixed oxides are detected. After exposed to reaction condition for ca. 8 h, the catalyst supports are mainly composed

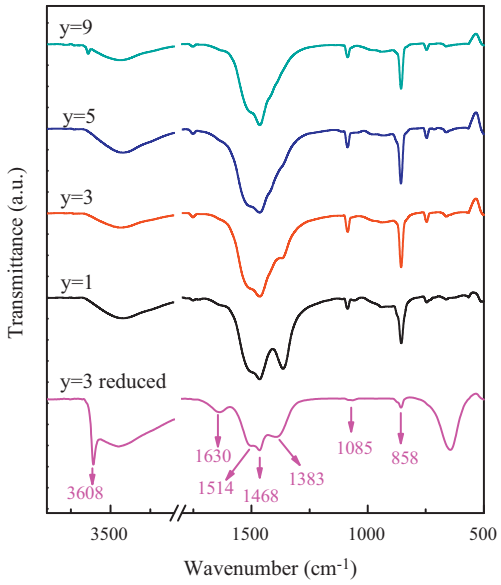

Fig. 5. FT-IR spectra of used Ir(3)Ca(y)/La_2O_3 catalysts (y = 1, 3, 5, 9) and reduced Ir(3)Ca(3)/La_2O_3 catalyst. Reaction condition: C/O = 1, S/C = 2, T = 650 °C, GHSV = 60,000 h^{-1}, reaction time of about 8 h.

of $La_2O_2CO_3$, because of the reaction between La_2O_3, $La(OH)_3$ and CO_2 in situ formed. It is similar to the case of as-prepared catalyst, that the higher content of Ca facilitates the transformation of monoclinic to hexagonal $La_2O_2CO_3$. This result shows that the working catalyst should be regarded as $La_2O_2CO_3$ supported Ir, instead of La_2O_3.

The evolution of support was well supported by FT-IR analysis. As shown in Fig. 5, in typical H_2-reduced catalyst, strong peaks at 3608 and 1630 cm^{-1} can be assigned as the bending and stretching modes of —OH in $La(OH)_3$. After reaction, these peaks disappear due to the formation of dioxycarbonates. According to literatures [41,49], the bands at 858 and 1468 cm^{-1} can be attributed to ν_2 and ν_3 modes of hexagonal $La_2O_2CO_3$, respectively. The bands at 1085 cm^{-1} are due to ν_1 modes of CO_3^{2-}. The bands at 1514 cm^{-1} are from the ν_3 modes of both hexagonal and monoclinic polymorphs. The bands at 1383 cm^{-1} can be assigned as ν_3 modes of monoclinic $La_2O_2CO_3$, which is weakened with increasing Ca content and completely vanishes in sample Ir(3)Ca(9)/La_2O_3, being consistent with the transformation of $La_2O_2CO_3$ from monoclinic to hexagonal type revealed by XRD.

The chemical state of Ir was investigated by XPS. Ir_{4f} XPS spectra of used catalysts are shown in Fig. 6 and Table 4. The XPS spectra were deconvoluted with constrains that the binding energy difference of $Ir_{4f7/2}$ and $Ir_{4f5/2}$ doublets is 2.9 eV and their area ratio is 4:3. We previously discovered that Ir can strongly interact with support to form Ir-doped $La_2O_2CO_3$, which co-exists with metallic Ir (Ir^0) in the course of OSR of ethanol [38]. The similar XPS signal of Ir doping the support, at binding energy of 62.5 eV for $Ir_{4f7/2}$, can be observed in Ir(3)/La_2O_3 catalyst after OSRG reaction. However, no Ir^0 was detected in Ir(3)/La_2O_3. The peak at 65.3 eV can be assigned as iridium oxides (Ir^{4+}). The addition of Ca changes the chemical state of Ir species markedly. With 5 wt% Ca, only Ir strongly interplaying with support ($Ir^{\delta+}$) can be detected in XPS. However, increasing Ca content up to 9% and above results in the formation of Ir^0, at ca. 61 eV. About 20% Ir^0 were detected in the samples with 15% Ca and Ir/$CaCO_3$. Taking into account the high conversion and H_2 selectivity over Ir(3)Ca(5)/La_2O_3, the $Ir^{\delta+}$ species strongly interacting with $La_2O_2CO_3$ can be rationalized as the working sites for OSRG reaction.

Table 4
Location of $Ir_{4f7/2}$ and percentage of Ir species in XPS spectra in Fig. 6.

	Ir(3)/La_2O_3	$y=3$	$y=5$	$y=9$	$y=15$	Ir(3)/$CaCO_3$
Ir^0 (eV/%)	/	/	/	60.8/5.4	61.7/22.6	60.5/20.7
$Ir^{\delta+}$ (eV/%)	62.5/87.9	62.9/75.8	63.2/100	63.3/94.6	63.2/77.4	63.4/79.3
Ir^{4+} (eV/%)	65.3/12.1	65.7/24.2	/	/	/	/

The varying chemical state of Ir with Ca doping suggests that the interaction between Ir and support is altered by the addition of Ca. H_2-TPR was used to evaluate the metal–support interaction (MSI). It should be noted that in the course of temperature ramping, carbonates and dioxycarbonates in support may decompose and contribute to the signal from TCD detector. Thus, two model catalysts, i.e. Ir/$La_2O_2CO_3$ and Ir/$CaCO_3$, were synthesized and tested with TPR technique. The $La_2O_2CO_3$ support was prepared by calcining La_2O_3 powder at 800 °C in CO_2 atmosphere. As shown in Fig. 7, Ir species are reduced at about 140 °C in Ir/$La_2O_2CO_3$. The peak centered at 750 °C can be attributed to the decomposition of $La_2O_2CO_3$. When Ir is loaded on $CaCO_3$, the reduction peak shifts toward higher temperature. The wide peak ranging from 300 to 600 °C can be attributed to the decomposition of $CaCO_3$. In IrCa/La_2O_3 catalysts, the dispersive peaks in the range from 300 to 550 °C are caused by the decomposition of $CaCO_3$ as modifier, which increase in intensity with the content of Ca. Compared to Ir/$La_2O_2CO_3$, the decomposition temperature of $La_2O_2CO_3$ shifts toward lower temperature, due to the lower structural stability of as-prepared catalyst. It is observed that the reduction temperature gradually increases as increases Ca content from 1% to 15%, indicating a strengthened MSI induced by Ca modification.

Fig. 8 shows HRTEM images of the used Ir(3)Ca(y)/La_2O_3 catalyst. Although the catalysts are low in specific surface area (Table 5), good dispersion of catalytic domains can be achieved due to the strong and unique MSI. In all the catalysts, clear fringes belonging to $La_2O_2CO_3$ support can be observed, indicating that the working catalysts are actually supported over dioxycarbonates, rather than oxides. Over Ir(3)/La_2O_3, the particle size is in the range from 1 to 5 nm and averaged at 2.4 ± 1.1 nm. The addition of Ca impressively reduces the particle size. As shown in Table 5, the average diameters of catalytic domains, identified as the dark dots in TEM images, decrease to 0.9 ± 0.4 nm as increase Ca content from 3 to 9 wt%. Further increasing Ca content to 15%, however, results in aggregation of catalyst particles, leading to the heterogeneity of particle size. It is rationalized by the segregation of $CaCO_3$ during preparing the catalyst (see Fig. 4a), because $CaCO_3$ is not capable to form highly dispersed Ir catalysts as evidenced by the TEM image of Ir/$CaCO_3$ (Fig. 8f). Above microscopic results explicitly demonstrate that the introduction of Ca modifier significantly tunes the catalyst dispersion, thereby one can expect the catalytic performance can be improved, as shown in Section 3.2.

3.4. Discussion on the effect of Ca

Some hetero-atoms, including Li, Pt and Eu, can be incorporated into the lattice of $La_2O_2CO_3$ [50,49,51]. It is well known that Ca can substitute for La sites in perovskites to induce oxygen vacancies [52,53]. Similarly, Ca may be incorporated into $La_2O_2CO_3$ to form doped dioxycarbonate, probably via substituting for La. This doped structure can be demonstrated by measuring the projected spatial elemental distribution in support and its impact on lattice

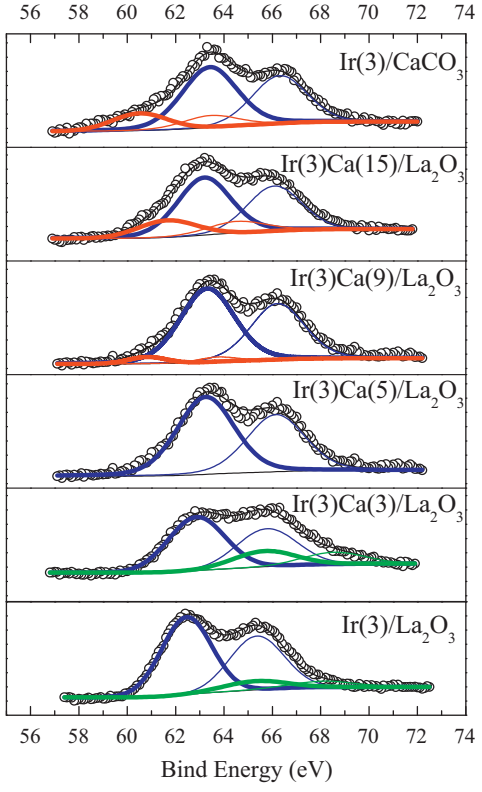

Fig. 6. Ir_{4f} XPS spectra of used Ir(3)Ca(y)/La_2O_3, Ir(3)/La_2O_3 and Ir(3)/$CaCO_3$ catalysts. $y=3, 5, 9, 15$. Reaction condition: C/O = 1, S/C = 2, T = 650 °C, GHSV = 60,000 h^{-1}, t = 8 h.

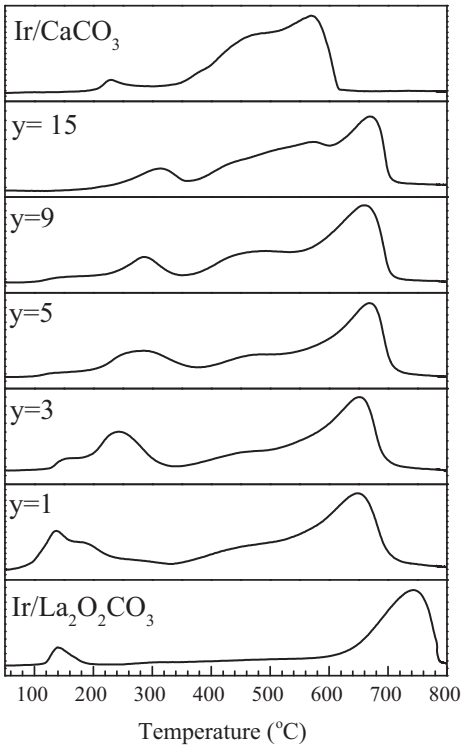

Fig. 7. H_2-TPR profiles of as-prepared Ir(3)Ca(y)/La_2O_3, Ir(3)/$La_2O_2CO_3$ and Ir(3)/$CaCO_3$ catalysts. $y=1, 3, 5, 9, 15$.

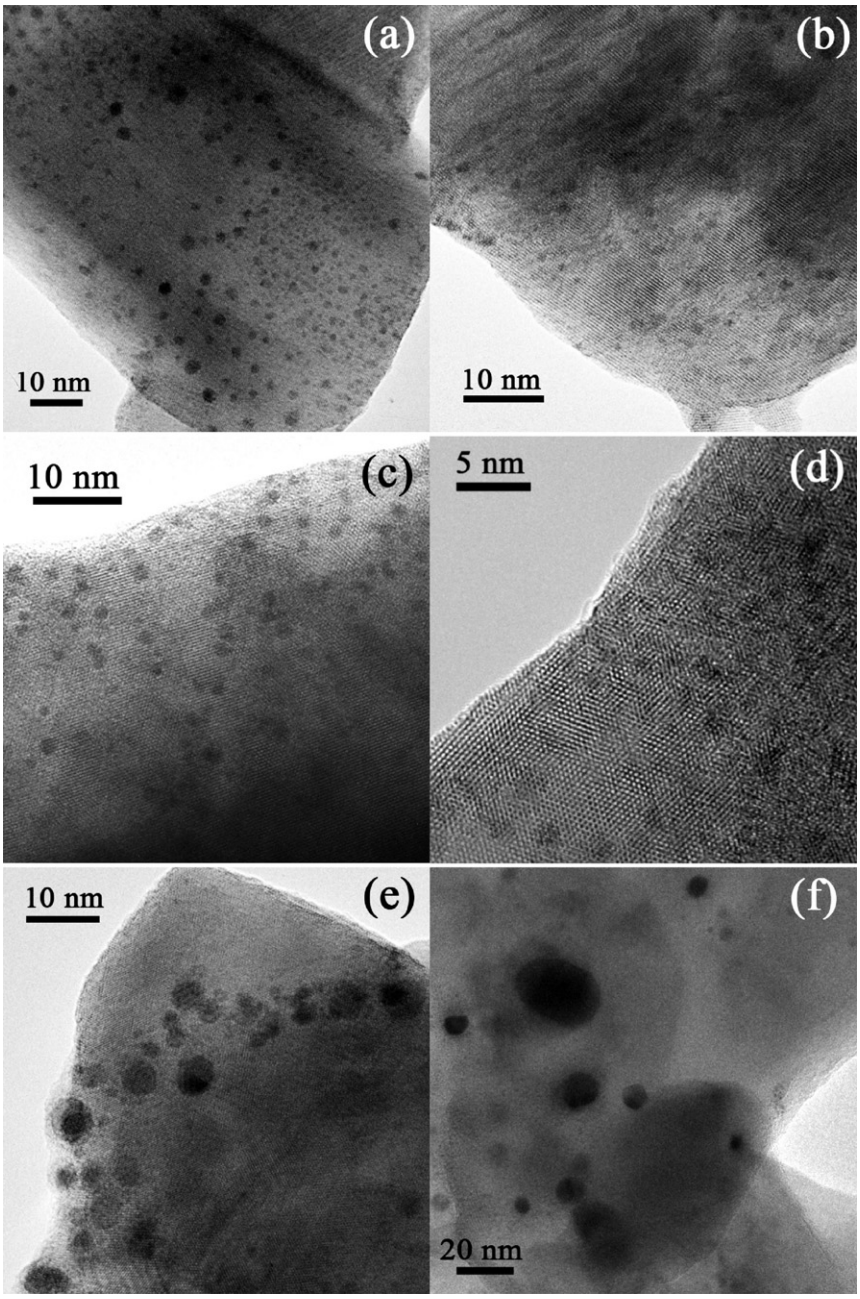

Fig. 8. TEM images of used (a) $Ir(3)/La_2O_3$, (b) $Ir(3)Ca(3)/La_2O_3$, (c) $Ir(3)Ca(5)/La_2O_3$, (d) $Ir(3)Ca(9)/La_2O_3$, (e) $Ir(3)Ca(15)/La_2O_3$ and (f) $Ir(3)/CaCO_3$ catalysts. Reaction condition: C/O = 1, S/C = 2, T = 650 °C, GHSV = 60,000 h^{-1}, 8 h.

parameters. As shown in Fig. 9, the EDS mapping result indicates that La, Ir and Ca elements are homogeneously distributed inside the catalyst particle, and no segregated Ca species, e.g. carbonates and oxides, can be observed as Ca amount is lower than 15% (see XRD evidences in Fig. 4). It can be explained by the doping of Ca on the atomic level. Additionally, the substitution of La by Ca results in the lattice shrinkage of $La_2O_2CO_3$ due to the smaller ionic radius of Ca. As shown in Fig. 10, when the Ir/La_2O_3 catalyst is modified by Ca, the (1 0 0), (1 0 1) and (1 0 2) reflections of hexagonal $La_2O_2CO_3$ markedly shift toward higher 2θ angle. For example, the (1 0 1) reflection shifts by about 0.06°, indicating a lattice shrinkage of 0.0192 Å. This shift of 2θ recovered as increased Ca amount to 15%, probably due to the segregation of calcium carbonates or oxides.

Table 5
Brunauer–Emmet–Teller specific surface area and average diameter of catalytic particles of used $Ir(3)Ca(y)/La_2O_3$.

Catalyst	$Ir(3)/La_2O_3$	y = 1	y = 3	y = 5	y = 9	y = 15	$Ir(3)/CaCO_3$
S_{BET} (m^2/g)	7.9	11.1	10.5	9.2	9.7	9.5	2.42
d[a] (nm)	2.4 ± 1.1	n.m.[b]	1.4 ± 0.9	1.4 ± 0.5	0.9 ± 0.4	n.m.[b]	n.m.[b]

[a] Measured by TEM statistics, used catalysts.
[b] Not measured.

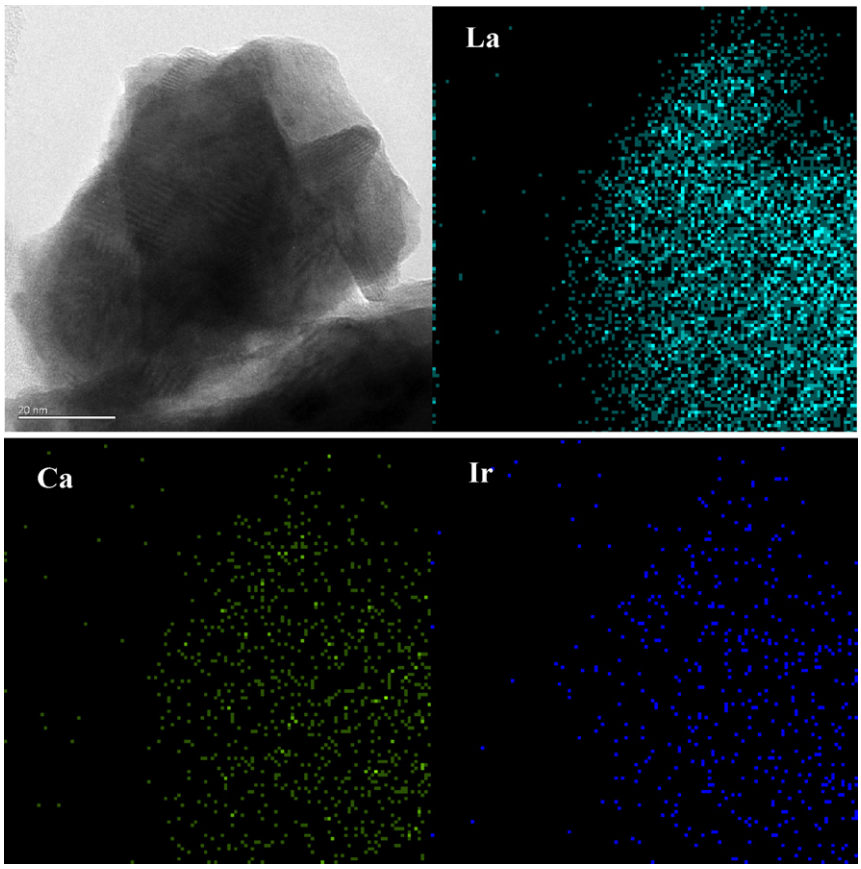

Fig. 9. TEM image and elemental distribution from EDS mapping of used Ir(3)Ca(9)/La_2O_3 catalyst. Reaction condition: C/O = 1, S/C = 2, T = 650 °C, GHSV = 60,000 h^{-1}, 8 h.

The doping of calcium induces structural defects of $La_2O_2CO_3$ via forming vacant anionic sites. La_2O_3 transforms toward $La_2O_2CO_3$ through the insertion of CO_2 into the layered $(La_2O_2)^{2+}$ units[54]. As some La^{3+} is replaced by Ca^{2+}, the exchange from O^{2-} to CO_3^{2-} between two adjacent $(La_2O_2)_n^{2n+}$ layers may become easier, since more anionic vacancies are available. Thus, the in situ formation of dioxycarbonates became faster as modified Ir/La_2O_3 with Ca, as revealed by XRD and FTIR in Figs. 4 and 5, while the decomposition temperature of $La_2O_2CO_3$ decreased as shown in TPR in Fig. 7. Additionally, the highly dispersed Ca sites in $La_2O_2CO_3$ endow the catalyst an enhanced basicity (see CO_2-TPD profiles in Fig. S3), since the lower electronegativity of Ca^{2+} than La^{3+} facilitates electron donation from the oxygen ions. On one hand, the improved basicity prevents coking over the catalyst surfaces; on the other hand, the fast insertion of CO_2 into layered $(La_2O_2)^{2+}$ units may speed up the reaction cycle ascribed by (2) and (3). Therefore, the Ca-doped catalyst displayed a markedly elongated lifetime without suffering from serious carbon deposition, as shown by the long-term stability test in Fig. 3. The resistance to coking resulted from Ca doping is so impressive that no any signal from carbon can be detected either in TEM or in the Raman spectrum of used catalyst, as shown in Fig. 11, taking Ir(3)Ca(5)/La_2O_3 as an example. Compared with the Raman spectrum of Ir(3)/La_2O_3, the G (1590 cm^{-1}) and D (1340 cm^{-1}) bands of carbon are totally absent in that of Ir(3)Ca(5)/La_2O_3, while the peaks from $CaCO_3$ (1082 cm^{-1}) and catalyst can be clearly observed (see Fig. S4 for the assignments of Raman peaks).

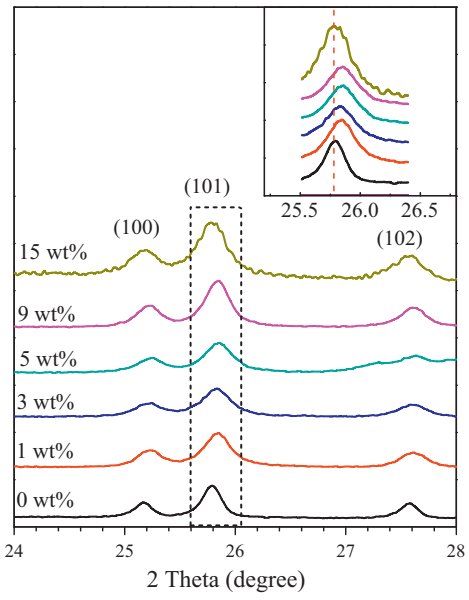

Fig. 10. High-resolution XRD patterns of used Ir(3)Ca(y)/La_2O_3 catalysts. The top right inset shows the details of (101) reflection of $La_2O_2CO_3$. Reaction condition: C/O = 1, S/C = 2, T = 650 °C, GHSV = 60,000 h^{-1}, 8 h.

The Ca dopant also alters the MSI. The evolution of interaction is clearly revealed by H_2-TPR shown in Fig. 7. The higher reduction temperatures of Ca doped catalysts are indicative of the stronger MSI. Such a strong MSI may lead to the more efficient electron transfer between metal and support. Due to the increased basicity, the electron donation from the oxygen ions toward catalyst domains may be enhanced, which results in the higher proportion of metallic Ir^0 on catalyst surfaces, as revealed by XPS analysis. It was noted that, with a proper Ca amount, 5% in this work, the metallic iridium or its oxides with higher valence state cannot be formed, besides the $Ir^{\delta+}$ strongly interacting with support. Recent advances on the

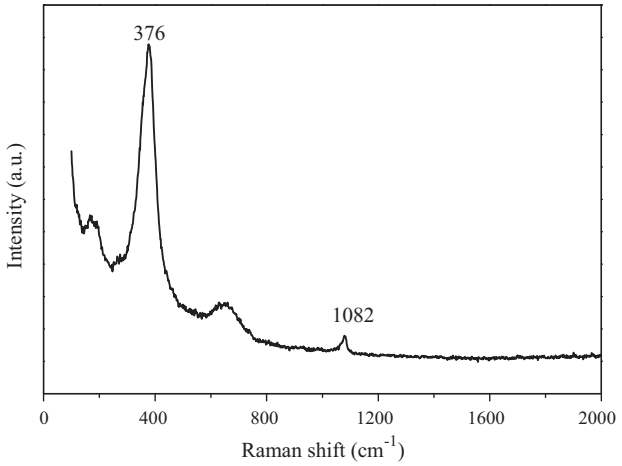

Fig. 11. Raman scattering spectrum of used Ir(3)Ca(5)/La_2O_3 catalyst. Reaction condition: C/O = 1, S/C = 2, T = 650 °C, GHSV = 120,000 h^{-1}, 8 h.

nature of reforming catalysts suggest that the working catalyst for reforming reaction may be cationic species, rather than metals as commonly recognized [55,56]. Our previous study [38] and the work from Bayram et al. [56] both indicate that metal and oxides co-exist on the surface of working catalysts for ethanol reforming, regardless of the initial state of metal. Co/Mg/Al hydrotalcite contains only traces of Co^0, due to the strong interaction between CoAl spinel particles as well as CoO with MgO, while Co^{2+} species are active for ethanol reforming [55]. The catalysis of ethanol reforming is dependent on valent state and coordination environment of metal species. Over Co/CeO_2, CoO is active, while Co_3O_4 is inactive for ethanol reforming [56]. On current stage, the exact molecular insight to the relationship between iridium coordination and OSRG reaction pathways is not yet known. However, our results evidenced that the Ca could facilitate the formation of highly active cationic sites as working catalysts, thereby improve the activity in OSRG reaction.

The strong MSI resulted in an impressively high dispersion of catalysts. Because of the fast formation and decomposition of dioxycarbonates, and the strong MSI, the aggregation of Ir species can be effectively suppressed, even under the harsh reaction conditions. Over Ir(3)Ca(9)/La_2O_3 catalyst, very small catalytic domains with an averaged diameter of 0.9 nm were observed. The resistance to sintering and coking synergistically maintains the high performance of IrCa/La_2O_3 catalysts in OSRG.

Conclusions

Ir/La_2O_3 catalysts are efficient in the OSRG reaction for hydrogen production. A parametric study showed that good activity and hydrogen selectivity can be achieved with 3 wt% loading of Ir at S/C = 2, C/O = 1 and 650 °C. However, the pristine Ir/La_2O_3 catalysts suffered from serious deactivation due to carbon deposition. Modifications with Na, Mg and Ca effectively improved the catalyst performance, especially in stability. The optimal catalytic results were obtained over the Ir(3)Ca(5–9)/La_2O_3 catalysts, which gave glycerol conversion approaching 90%, hydrogen selectivity higher than 70% and stability up to 100 h. It was found that Ca was homogenously doped into $La_2O_2CO_3$, in situ formed during the OSRG reaction via the reaction between La_2O_3 and CO_2. The functions of Ca dopant were rationalized as:

i) increasing the basicity, thereby preventing the catalyst from coking;
ii) inducing structural defects of $La_2O_2CO_3$, which speeds up the dynamic formation and decomposition of $La_2O_2CO_3$ as support, thereby prevent the catalytic domains from sintering;
iii) tuning the metal–support interaction, which leads to the formation of homogenously dispersed Ir species with strong interaction with $La_2O_2CO_3$ support and facilitates the high activity in OSRG.

Acknowledgements

This work was supported by the National High Technology Research and Development Program of China(863 Program, No. 2009AA05Z102), the Natural Science Foundation of China (No. 20176094), the Guangdong Provincial Science and Technology Project (No. 2010B050200003) and the Fundamental Research Funds for the Central Universities of China (Nos. 2009zm0246 2012ZZ0039).

Appendix A. Supplementary data

Supplementary data associated with this article can be found, in the online version, at http://dx.doi.org/10.1016/j.apcatb.2012.08.003.

References

[1] A.C.C. de Souza, J.L. Silveira, Renewable and Sustainable Energy Reviews 15 (2011) 1835–1850.
[2] C.H.C. Zhou, J.N. Beltramini, Y.X. Fan, G.Q.M. Lu, Chemical Society Reviews 37 (2008) 527–549.
[3] P.D. Vaidya, A.E. Rodrigues, Chemical Engineering & Technology 32 (2009) 1463–1469.
[4] S. Adhikari, S.D. Fernando, A. Haryanto, Energy Conservation & Management 50 (2009) 2600–2604.
[5] S. Adhikari, S.D. Fernando, S.D.F. To, R.M. Bricka, P.H. Steele, A. Haryanto, Energy & Fuels 22 (2008) 1220–1226.
[6] I.N. Buffoni, F. Pompeo, G.F. Santori, N.N. Nichio, Catalysis Communications 10 (2009) 1656–1660.
[7] T. Hirai, N. Ikenaga, T. Miyake, T. Suzuki, Energy & Fuels 19 (2005) 1761–1762.
[8] N.J. Luo, K. Ouyang, F.H. Cao, T.C. Xiao, Biomass & Bioenergy 34 (2010) 489–495.
[9] T. Valliyappan, N.N. Bakhshi, A.K. Dalai, Bioresource Technology 99 (2008) 4476–4483.
[10] A.J. Byrd, K.K. Pant, R.B. Gupta, Fuel 87 (2008) 2956–2960.
[11] V.M. Daskalaki, D.I. Kondarides, Catalysis Today 144 (2009) 75–80.
[12] S. Adhikari, S. Fernando, A. Haryanto, Catalysis Today 129 (2007) 355–364.
[13] S. Adhikari, S.D. Fernando, A. Haryanto, Renewable Energy 33 (2008) 1097–1100.
[14] T. Valliyappan, D. Ferdous, N.N. Bakhshi, A.K. Dalai, Topics in Catalysis 49 (2008) 59–67.
[15] E.A. Sanchez, M.A. D'Angelo, R.A. Comelli, International Journal of Hydrogen Energy 35 (2010) 5902–5907.
[16] V. Chiodo, S. Freni, A. Galvagno, N. Mondello, F. Frusteri, Applied Catalysis A: General 381 (2010) 1–7.
[17] A. Iriondo, V.L. Barrio, J.F. Cambra, P.L. Arias, M.B. Guemez, R.M. Navarro, M.C. Sanchez-Sanchez, J.L.G. Fierro, Topics in Catalysis 49 (2008) 46–58.
[18] A. Iriondo, V.L. Barrio, J.F. Cambra, P.L. Arias, M.B. Guemez, M.C. Sanchez-Sanchez, R.M. Navarro, J.L.G. Fierro, International Journal of Hydrogen Energy 35 (2010) 11622–11633.
[19] A. Iriondo, V.L. Barrio, J.F. Cambra, P.L. Arias, M.B. Guemez, R.M. Navarro, M.C. Sanchez-Sanchez, J.L.G. Fierro, Catalysis Communications 10 (2009) 1275–1278.
[20] L.P.R. Profeti, E.A. Ticianelli, E.M. Assaf, International Journal of Hydrogen Energy 34 (2009) 5049–5060.
[21] D. Karthikeyan, G.S. Shin, D.J. Moon, J.H. Kim, N.C. Park, Y.C. Kim, Journal of Nanoscience and Nanotechnology 11 (2011) 1443–1446.
[22] C.K. Cheng, S.Y. Foo, A.A. Adesina, Catalysis Communications 12 (2010) 292–298.
[23] E.B. Pereira, P.R. de la Piscina, N. Homs, Bioresource Technology 102 (2011) 3419–3423.
[24] L. He, J.M.S. Parra, E.A. Blekkan, D. Chen, Energy & Environmental Science 3 (2010) 1046–1056.
[25] D.A. Simonetti, E.L. Kunkes, J.A. Dumesic, Journal of Catalysis 247 (2007) 298–306.
[26] D.C. Rennard, J.S. Kruger, L.D. Schmidt, ChemSusChem 2 (2009) 89–98.
[27] N.J. Luo, X.W. Fu, F.H. Cao, T.C. Xiao, P.P. Edwards, Fuel 87 (2008) 3483–3489.
[28] A.O. Menezes, M.T. Rodrigues, A. Zimmaro, L.E.P. Borges, M.A. Fraga, Renewable Energy 36 (2011) 595–599.

[29] P.J. Dauenhauer, J.R. Salge, L.D. Schmidt, Journal of Catalysis 244 (2006) 238–247.
[30] D.C. Rennard, J.S. Kruger, B.C. Michael, L.D. Schmidt, Industrial & Engineering Chemistry Research 49 (2010) 8424–8432.
[31] A. Gallo, C. Pirovano, M. Marelli, R. Psaro, V. Dal Santo, Chemical Vapor Deposition 16 (2010) 305–310.
[32] A. Gallo, C. Pirovano, P. Ferrini, M. Marelli, R. Psaro, S. Santangelo, G. Faggio, V. Dal Santo, Applied Catalysis B: Environmental 121 (2012) 40–49.
[33] B.C. Zhang, X.L. Tang, Y. Li, Y.D. Xu, W.J. Shen, International Journal of Hydrogen Energy 32 (2007) 2367–2373.
[34] G.X. Yang, H. Yu, F. Peng, H.J. Wang, J. Yang, D.L. Xie, Renewable Energy 36 (2011) 2120–2127.
[35] A.J.H.M. Kock, P.K. de Bokx, E. boellaard, W. Klop, J.W. Geus, Journal of Catalysis 96 (1985) 468–480.
[36] D. Duprez, M.C. Demicheli, P. Marecot, J. Barbier, O.A. Ferretti, Journal of Catalysis 124 (1990) 324–335.
[37] S. Tang, L. Ji, J. Lin, H.C. Zeng, K.L. Tan, K. Li, Journal of Catalysis 194 (2000) 424–430.
[38] H.Q. Chen, H. Yu, F. Peng, H.J. Wang, J. Yang, M.Q. Pan, Journal of Catalysis 269 (2010) 281–290.
[39] T. Levan, M. Che, J.M. Tatibouet, M. Kermarec, Journal of Catalysis 142 (1993) 18–26.
[40] A.N. Fatsikostas, D.I. Kondarides, X.E. Verykios, Catalysis Today 75 (2002) 145–155.
[41] R.P. Turcotte, J. Sawyer, L. Eyring, Inorganic Chemistry 8 (1969) 238–246.
[42] K.K. Bando, K. Soga, K. Kunimori, H. Arakawa, Applied Catalysis A: General 175 (1998) 67–81.
[43] Q. Miao, G.X. Xiong, S.S. Sheng, X.X. Guo, Reaction Kinetics and Catalysis Letters 62 (1997) 363–370.
[44] J.S. Chang, S.E. Park, J.W. Yoo, J.N. Park, Journal of Catalysis 195 (2000) 1–11.
[45] T. Osaki, T. Mori, Journal of Catalysis 204 (2001) 89–97.
[46] J. Juan-Juan, M.C. Roman-Martinez, M.J. Illan-Gomez, Applied Catalysis A: General 264 (2004) 169–174.
[47] H. Jeong, K.I. Kim, D. Kim, I.K. Song, Journal of Molecular Catalysis A: Chemical 246 (2006) 43–48.
[48] Z. Xu, Y. Li, J. Zhang, L. Chang, Chinese Journal of Catalysis 18 (1997) 3.
[49] S. Irusta, L.M. Cornaglia, E.A. Lombardo, Materials Chemistry and Physics 86 (2004) 440–447.
[50] J.P. Attfield, G. Férey, Journal of Solid State Chemistry 82 (1989) 132–138.
[51] G.G. Li, C. Peng, C.M. Zhang, Z.H. Xu, M.M. Shang, D.M. Yang, X.J. Kang, W.X. Wang, C.X. Li, Z.Y. Cheng, J. Lin, Inorganic Chemistry 49 (2010) 10522–10535.
[52] N.H. Batis, P. Delichere, H. Batis, Applied Catalysis A: General 282 (2005) 173–180.
[53] S.Q. Chen, H. Wang, Y. Liu, International Journal of Hydrogen Energy 34 (2009) 7995–8005.
[54] A. Olafsen, H. Fjellvag, Journal of Materials Chemistry 9 (1999) 2697–2702.
[55] R. Espinal, E. Taboada, E. Molins, R.J. Chimentao, F. Medina, J. Llorca, RSC Advances 2 (2012) 2946–2956.
[56] B. Bayram, I.I. Soykal, D. von Deak, J.T. Miller, U.S. Ozkan, Journal of Catalysis 284 (2011) 77–89.